Human Powered Vehicle Challenge

By
Matt Gerlich, Alex Hawley, Phillip Kinsley,
Heather Kutz, Kevin Montoya, Erik Nelson
Team 9

Engineering Analysis

Document

Submitted towards partial fulfillment of the requirements for
Mechanical Engineering Design I – Fall 2013

Department of Mechanical Engineering
Northern Arizona University
Flagstaff, AZ 86011

TABLE OF CONTENTS

1.0 INTRODUCTION

For the 2014 Human Powered Vehicle Challenge (HPVC) Team 9 will design, analyze, and construct a vehicle that meets the requirements given by the American Society of Mechanical Engineers (ASME) and the project's client, Perry Wood. To analyze the vehicle, the project was divided into six subsections. These sections include: frame, fairing, steering, drivetrain, ergonomics, and innovation. For each subsection a set of analysis was computed either mathematically or numerically. Each analysis task completed will be explained in detail with the results presented. This paper will also give an update on the project's overall progress.

2.0 PROJECT DESCRIPTION

Team 9 will design and build a human powered vehicle to compete in the HPVC, held by ASME. The competition consists of a design event, a sprint or drag event, an endurance race, and an innovation presentation. The sponsors for this project are Perry Wood, the NAU ASME advisor, and ASME. A goal statement was generated that states the team will "Design a human powered vehicle that can function as an alternative form of transportation." This provides the team a large scope while brainstorming ideas within their sections. A few objectives the team has for the vehicle includes: speed, aerodynamics, and maneuverability.

3.0 ANALYSIS

3.1 FRAME

The frame section of the analysis was broken into three separate sections: the main center tube, the outriggers, and the roll bar. Bending resistances were examined for the center tube because they were deemed important. The outriggers and the roll bar were both analyzed for stresses and deflections. Along with the above analysis, all the weights were compared to find the most optimal strength to weight ratio for each part.

Initially five different configurations were analyzed by hand. These configurations include: 2" diameter aluminum with 0.125" thickness, 1.75" diameter aluminum with 0.125" thickness, 1.5"x1.5" square aluminum with 0.125" thickness, 2"x1" rectangular aluminum with 0.125" thickness, and 1.5" diameter steel with 0.058" thickness, which was used as a baseline comparison because it was used on NAU's Human Powered Vehicle in the past. All of the aluminum being analyzed is 6061 T6 and the steel is 4130.

The first analysis task was to find resistance to deflection for the center tube for each configuration. The frame was simplified to a simply supported beam with an applied load to the top. From this, a free body diagram was constructed, as seen in Figure 1. The deflection for this case can be found using the following equation [1]:

$$y = \frac{Fbx}{6EIL}(x^2 + b^2 - l^2) \qquad (1)$$

Where:

F= applied force [lb]
b= distance from B to force [in]
x= distance from A to force [in]
L= length of beam [in]
E= modulus of elasticity [ksi]
I= moment of inertia [in^4]

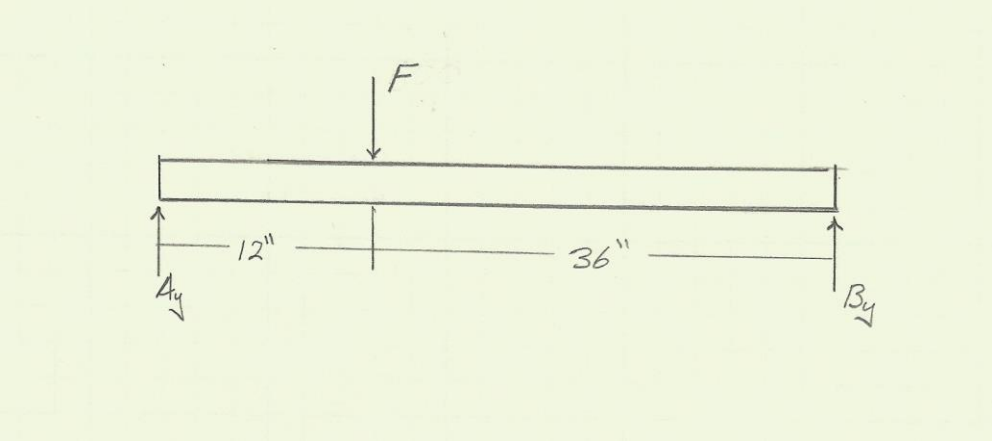

Figure 1- Frame Free Body Diagram

The modulus of elasticity for 6061 T6 aluminum is 10,400 ksi, and for 4130, the modulus of elasticity is 29,000 ksi [2]. The moment of inertia was found for the rectangular and square cross sections using the following equation:

$$I_{rec} = \frac{b_1 h_1^3 - b_2 h_3^3}{12} \quad (2)$$

Where:

b_1= outside base [in]
b_2= inner base [in]
h_1= outer height [in]
h_2= inner height [in]

To find the moment of inertia for the circular cross sections the following equation was used:

$$I_{cir} = \pi \frac{d_o^4 - d_i^4}{64} \quad (3)$$

Where:

d_o= outer diameter [in]
d_i= inner diameter [in]

The same deflection calculations were performed on the outriggers. These were simplified into a cantilever beam with an applied load to the end. The free body diagram for this can be seen below:

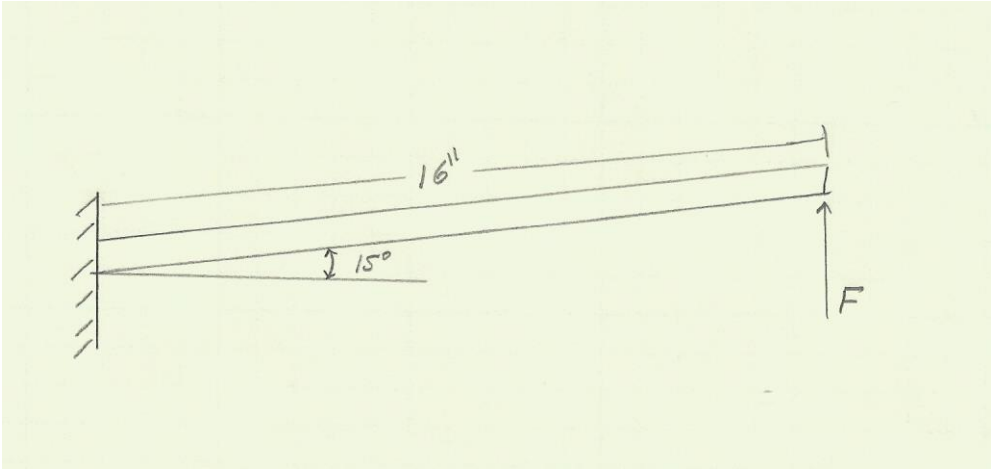

Figure 2- Outrigger Free Body Diagram

The deflection for this scenario is given by the following equation:

$$y = \frac{PL^3}{3EI} \tag{4}$$

Where:

P= Fcos(15°) [lbs]

In addition to this, the bending stresses on the outriggers also needed to be calculated. To accomplish this, the following equation was used:

$$\sigma = \frac{Mc}{I} \tag{5}$$

Where:

c= distance from neutral axis to extreme fiber [in]
M= moment [lb-in]

Stress concentrations were also taken into account for the outrigger connection to the frame. To find the stress concentration the following equations were used:

$$K_f \approx 1 + q(k_t - 1) \tag{6}$$

Where:

q= notch sensitivity
k_t= theoretical stress concentration factor

$$\sigma_{max} = K_f \sigma_{nom} \tag{7}$$

K_t and q were approximated for aluminum using tables [2]. K_f was found to be 1.54 for the square geometry and 1.45 for the round geometry.

The results from these calculations are given in Table 1 below. The force applied on the main tube was 600lb, and the force on the edge of the outriggers was 275lb, measured from accelerometer tests, seen in Appendix A. The deflections were also calculated for a lateral load applied in the z-direction of the material. The lateral load for the main tube was 300lb and the lateral load for the outriggers was 100lb.

Table 1- Hand Calculation Results

Configuration	1.5”ODx.058”ST	2”ODx0.125”AL	1.5”x1.5”X0.125”AL	1.75”ODx0.125”AL	2”x1”x0.125”AL
Main Tube Deflection [in]	0.392	0.230	0.342	0.353	0.225
Outrigger Deflection [in]	0.183	0.107	0.159	0.165	0.105
Main Tube Lateral Deflection [in]	0.196	0.115	0.171	0.176	0.356
Outrigger Lateral Deflection [in]	0.069	0.040	0.060	0.062	0.125
Weight [lb/in]	0.075	0.071	0.066	0.061	0.066
Outrigger Stress [psi]	46598	13077	14593	17551	12813
Outrigger Stress Max [psi]	55917	18961	22473	25448	19732

With aluminum having a yield strength of 40,000 psi [2], none of the configurations failed, but from this data it was clear that the 1.5”x1.5”x0.125” square tube, 2”x0.125” circular tube, and the 1.75”x0.125” circular tube were the best choices to continue analysis with. SolidWorks models were constructed for the three configurations and finite element analysis was used on each configuration to compare to the hand calculations.

The results of the outrigger calculations for the 1.5”x1.5” square tubing is displayed in Figures 3 and 4. The max stress on the outrigger was 16,309 psi, and the max deflection was calculated to be 0.159”. The stress number is in between the nominal and max calculated by hand, and the deflection is exactly the number calculated by hand. Therefore, these numbers appear to be valid.

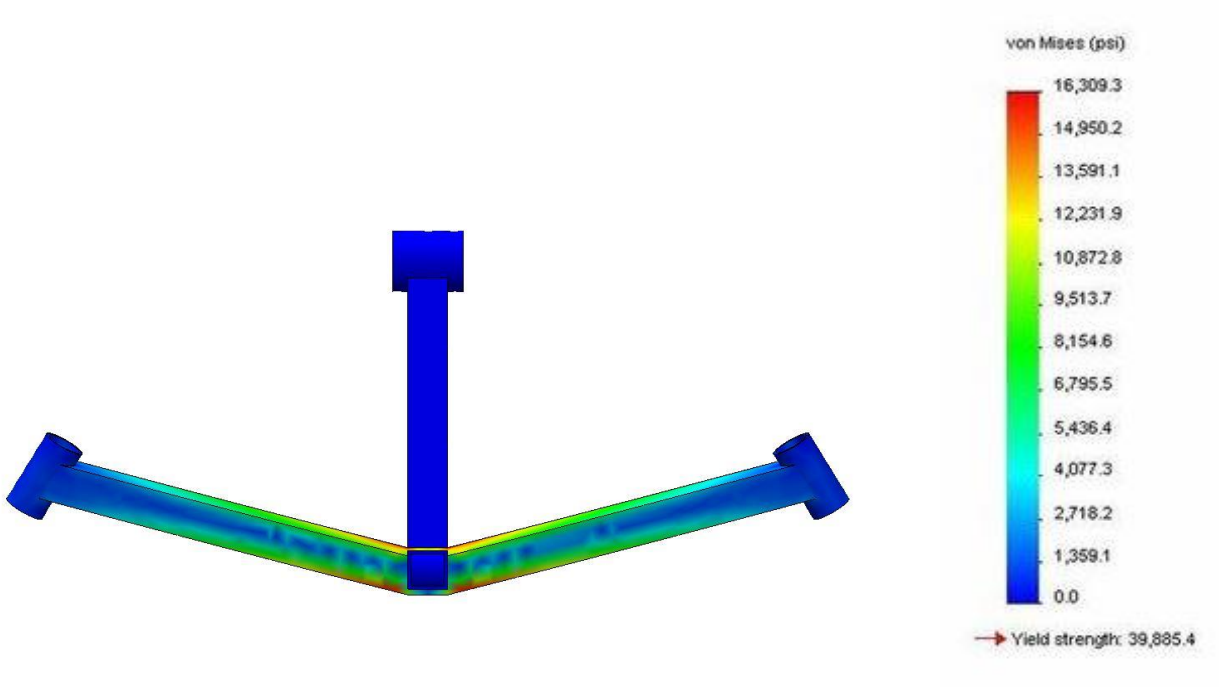

Figure 3- Square Outrigger Stress

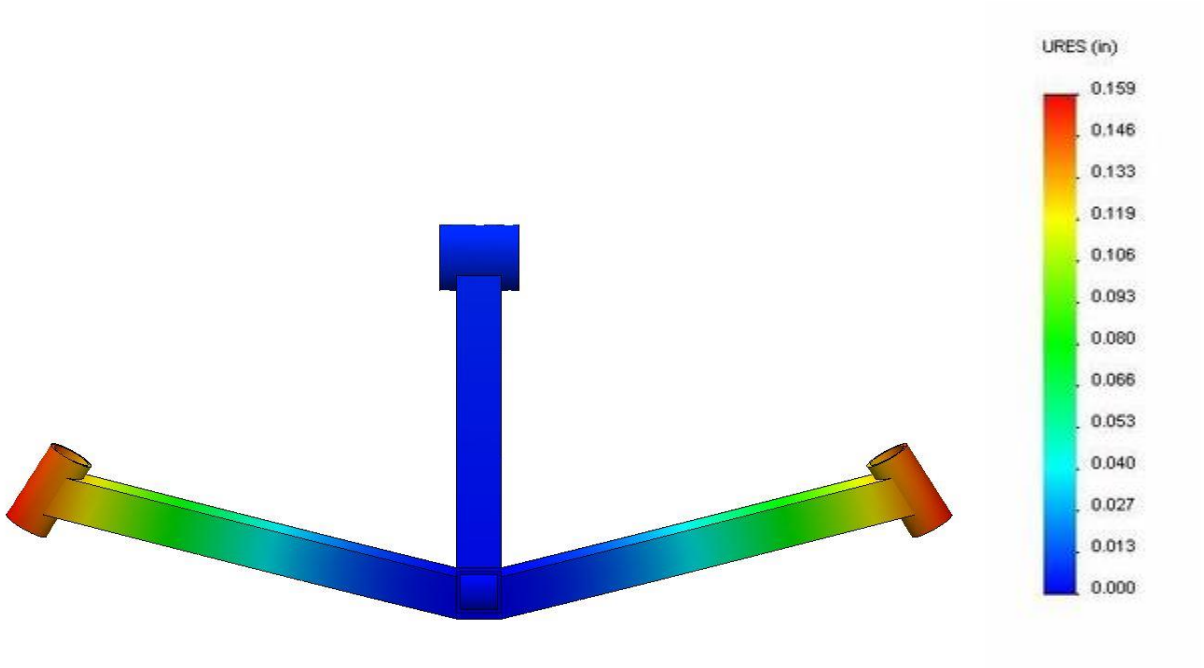

Figure 4- Square Outrigger Deflection

The finite element analysis results for the 1.75” circular tubing outriggers is displayed in Figures 5 and 6. The max stress the outrigger experienced in this test was 21,897 psi, and the maximum deflection was 0.139”. The stress, again, fell between the nominal and maximum calculated values, and the deflection was slightly less than the value calculated by hand.

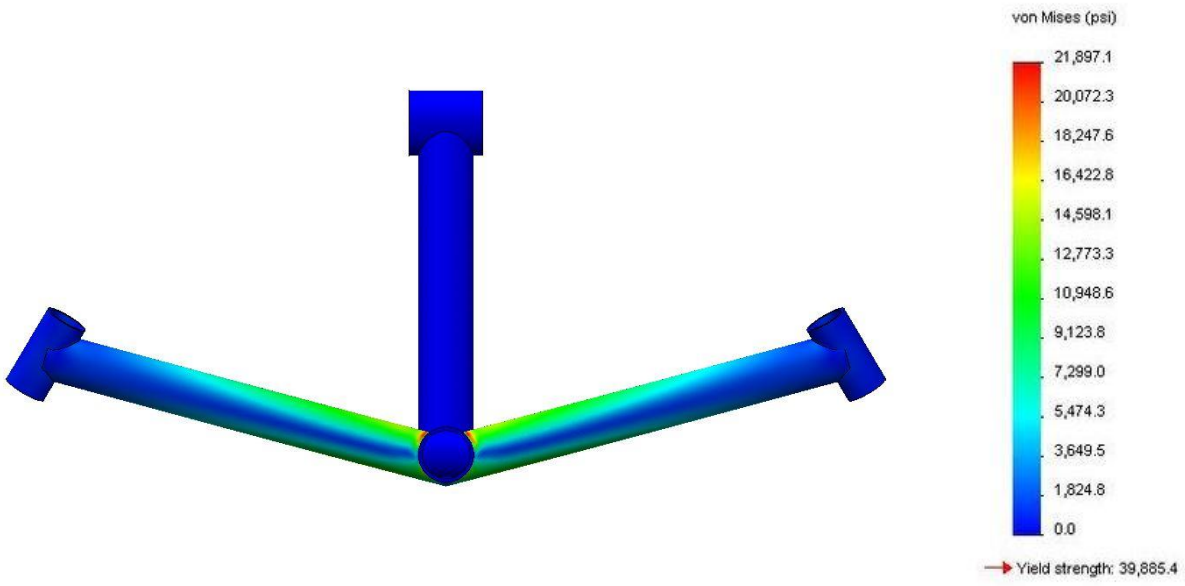

Figure 5- Circular Outrigger Stress

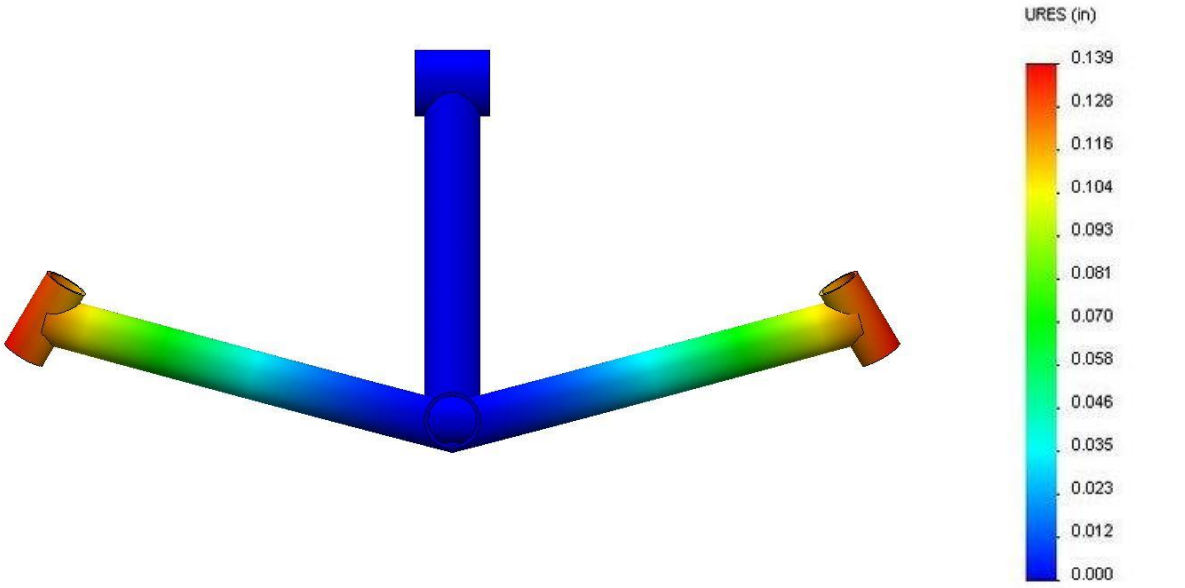

Figure 6- Circular Outrigger Deflection

The roll bar was also tested in three separate loading configurations: the max driving load of 225lb at the wheel from the accelerometer readings, 600lb top load, and 300lb side load as per the competition requirements.

The 225lb load at the wheel test can be seen in Figure 7. This test resulted in a maximum stress of 13,600 psi.

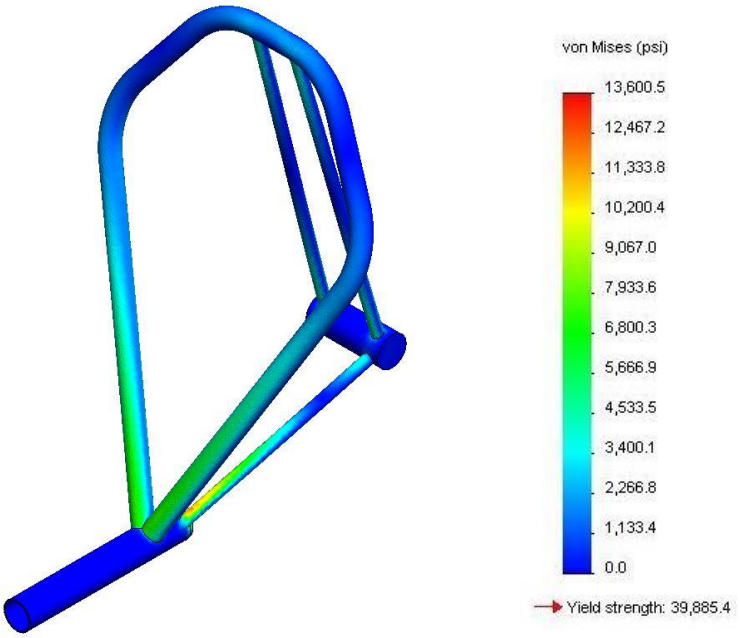

Figure 7- Driving Load Roll Bar Stress

The next test was the 600lb top load applied at an angle of 12° from vertical. The maximum stress experienced was 25,926psi, and the overall deformation was 0.607”, which is well below the competition requirements of 2”. This deflection can be seen in Figure 8 below:

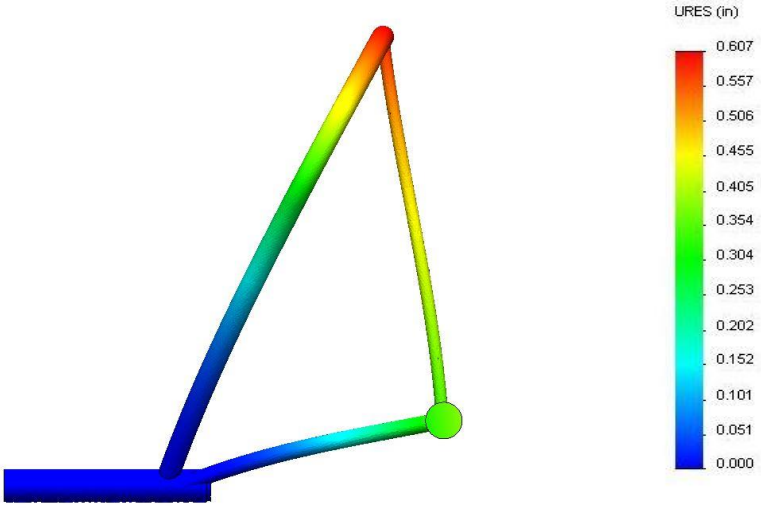

Figure 8-Top Load Roll Bar Deflection

With the 300lb load applied at shoulder height, the roll bar experienced a maximum stress of 20,171 psi and a maximum deflection of 0.511”, again below the competition requirement of less than 1.5”. This deflection can be seen in the Figure 9 below:

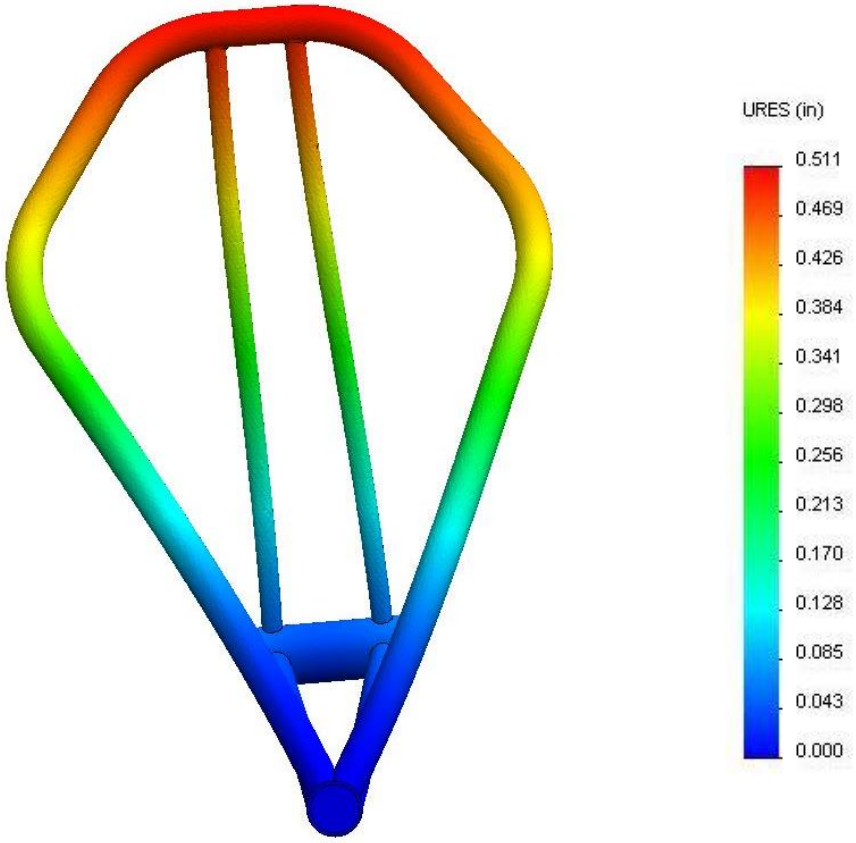

Figure 9- Side Load Roll Bar Deflection

A summary of the comparisons between the finite element analysis and the hand calculations is given below in Table 2. Since several assumptions were made to perform the calculations, and all of these results are close to what was calculated, these results appear to be accurate.

Table 2- FEA vs. Calculated Results

Configuration	1.5x1.5X0.125AL	1.75ODx0.125AL
Calculated Deflection [in]	0.159	0.165
FEA Deflection [in]	0.159	0.139
Calculated Nominal Stress [psi]	14593	17551
Calculated Max Stress [psi]	22473	25448
FEA Stress [psi]	16309	21897

Based on the above results the team will be selecting the square 1.5”x1.5”x0.125” aluminum configuration. The square configuration provides better resistances to deflections than the baseline 1.5” diameter steel tube, and it has less stress on the outriggers than the circular outrigger. The square shape also simplifies the manufacturing and seat integration considerably. The square configuration center tube will also be lighter than the circular configuration.

3.2 ERGONOMICS

In order to determine the position of the rider in the vehicle, the team conducted several tests using a stationary recumbent bicycle. The tests were done on a Monday, Wednesday, and Friday of one week and each team member was positioned at a different angle (shown in Figure 10) each day. These angles were 115°, 122°, and 130°. Each rider had to complete a ten-minute warm-up, followed by a one-minute sprint and a three-minute endurance test. The tests allowed the team to measure max and average power, max and average cadence, average heart rate, and energy expended. The data collected in these tests can be seen in Appendix D.

Figure 10- Rider Position Angle

Figure 11 shows the max power of each team member’s three tests for the one-minute sprint. The results show that an angle of 130° was the most common for having the highest max power among the team members. Since the riders vary significantly in weight, the power to weight ratio was calculated. The 130° angle had the highest average ratio.

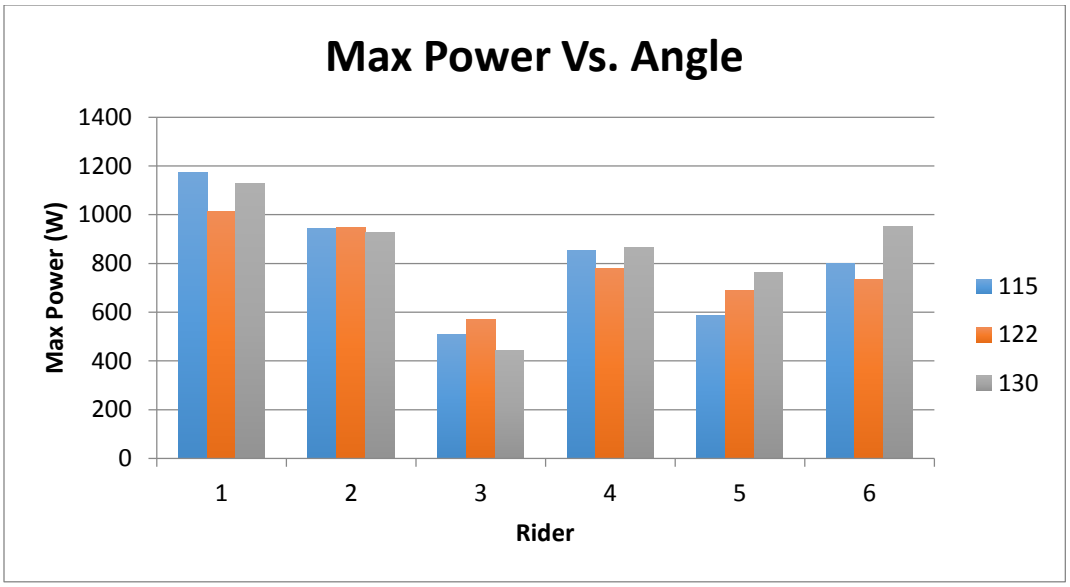

Figure 11- Max Power at Various Angles

Figure 12 shows the average power of each team member's three tests for the three-minute endurance test. These results show that an angle of 122° was the most common for having the highest average power among the team members. An angle of 122° also had the highest average for the power to weight ratio.

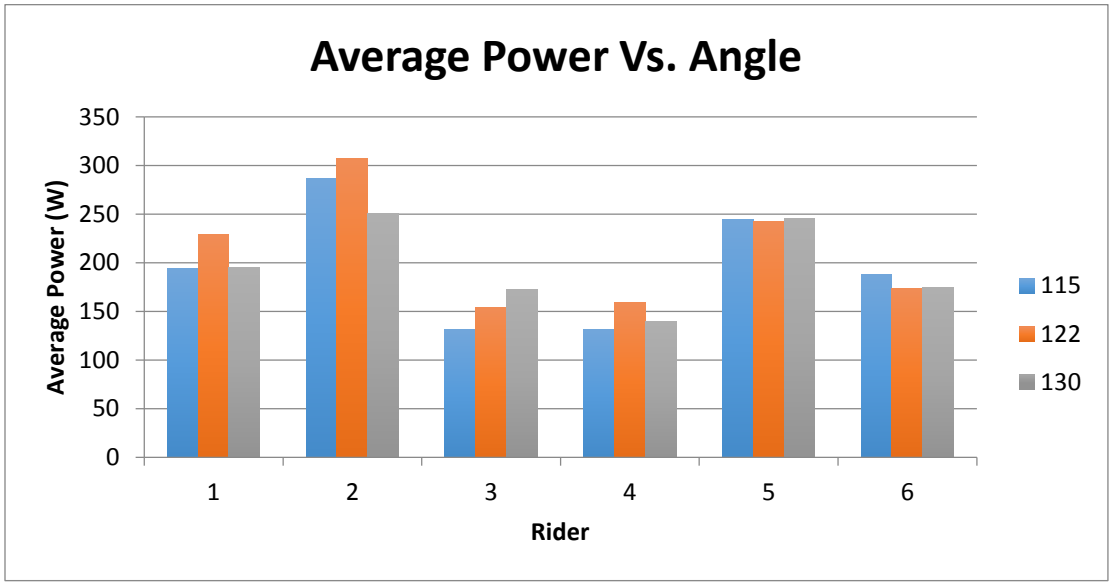

Figure 12- Average Power at Various Angles

There are several factors that could have affected the tests, such as the energy level, food and sleep. These could affect the amount of effort the rider strives to put forth during the test. The team did their best to keep each test as controlled as possible. The team has concluded that

many more tests would need to be done to obtain a more accurate result, but these tests give the team a general range of seat positions that can be chosen for optimal power output.

After discussion, the team chose an angle of 122° for the final rider position. It was decided that the endurance test was more important than the sprint test because the vehicle is meant to be used in urban environments, which includes farther distances than a typical sprint. Visibility is also an important factor. By choosing a less steep angle, the rider will be able to see over the pedals and therefore, creates a safer vehicle.

3.3 FAIRING

To ensure that the team will have a fast vehicle, the fairing must move the air around it in such a way that the minimum amount of force is applied to the vehicle. The possibilities are endless towards designing a fairing, but the team has decided to look at The Axe's fairing from last year, and create a design stemmed from that. The length, width, and height are all important in designing a fairing and those variables will be changed to see the relationships between them. While the fairing model has other components in the design, like the airfoil equations seen below, they will be kept constant [3]. For the length of the vehicle, a starting length of 96 inches was chosen from the dimensions of the test rig used in the rider position study. From there, the size was increased from 96 inches to 108 inches with six inch increments. The minimum width was based on the largest shoulder width of a team mate. The smallest width started at 18 inches, increasing to 24 inches, with increments of two inches. Finally, the height was based on the angles mentioned previously in the ergonomics section with the tallest team member's geometry. The angles were converted to the different heights of 33, 37, and 39 inches. The variables were applied and created thirty six different fairing designs to be analyzed.

$$y_t = \frac{tc}{0.2}\left[.2969\left(\sqrt{\frac{x}{c}}\right) - .1260\left(\frac{x}{c}\right) - .3516\left(\frac{x}{c}\right)^2 + .2843\left(\frac{x}{c}\right)^3 - .1015\left(\frac{x}{c}\right)^4\right] \qquad (8)$$

When setting up the computational fluid dynamics, CDF, in SolidWorks®, assumptions had to be made to retrieve results. To begin, the fluid was air at a temperature of 68° Fahrenheit and was assumed to have laminar flow. The velocity was equal to 704 inches per second, which is forty miles per hour, same as the team's goal. The body had a roughness of .012 microns, which is equivalent to the surface of aluminum. This can be assumed because the epoxy matrix in the carbon fiber composite takes on the surface characteristics of its mold. Lastly, the boundaries for the fluid analysis were 300 inches in length, 68 inches in width, and 96 inches in height.

Prior to completing the analysis the team had hypothesized that a fairing with the smallest width, height, and length would produce the lowest coefficient of drag, C_d. In the equation seen below, it does seem intuitive for the C_d to be low if the area is low.

$$C_d = \frac{2F_d}{\rho A V^2} \quad (9)$$

Analysis began with the length being changed at every width and height combination. To change the length of the fairing, the "c" variable as well as the "t" variable in the air foil equation had to be changed. The "t" variable had to be changed because it is a function of "c". Once completed, the results favored a fairing with a length of 102 inches with 50% of the data points having the lowest C_d, in each category. A length of 108 inches came in second with 42%, while the length of 96 inches had only 8% with the lowest C_d. From these results it is noted that the general fairing design has a lower C_d at longer lengths. See Appendix C for the data results.

Next, the width was changed at every length and height combination. Like the length, the airfoil equation constant, "t", had to be changed to modify the width along the body of the fairing. From the results of the CFD analysis, the width of 22 inches had 44% of the data points with the lowest C_d in each category. The widths of 20 and 18 inches had the same percent of 22%, while the widest width of 24 inches had 11% of the lowest C_d data points. As mentioned before, the team had hypothesized that the smallest width would produce the smallest C_d. The results from the CFD show that the fairing with one of the largest widths produces the lowest C_d. See Appendix C for the data results.

Lastly, the height was changed at every length and width combination. Unlike the previous two dimensions, the upper and lower splines were changed to modify the height. The height of 33 inches produced the most results with the lowest C_d. It scored better than the heights of 37 and 39 inches ten out of the twelve scenarios. The heights of 37 and 39 inches both had 8% of the data points below the C_d. In conclusion, a shorter fairing results in a lower C_d.

As mentioned above, the angle of the rider was chosen to be 122°, which correlates to the height of 37 inches. Table 3, shown below, consists of all of the options relating to the height of 37 inches. The shape with the lowest coefficient of drag is that of the size 108L, 22W, and 37H. The closet option after that would be a fairing of the size 102L, 18W, and 37H.

Table 3– Coefficient of Drag Comparison

Length (in)	Width (in)	Height (in)	Speed (in/s)	Force (lbf)	Area (in^2)	Cd
96	18	37	704	0.5995	681.54	0.038
96	20	37	704	0.5132	716.58	0.031
96	22	37	704	0.5417	760.07	0.031
96	24	37	704	0.6170	803.72	0.033
102	18	37	704	0.4110	670.37	0.026
102	20	37	704	0.4957	702.1	0.030
102	22	37	704	0.5659	753.55	0.032
102	24	37	704	0.5126	790.64	0.028
108	18	37	704	0.5400	670.51	0.035
108	20	37	704	0.4895	701.49	0.030
108	22	37	704	0.4376	740.06	0.025
108	24	37	704	0.5767	788.48	0.032

In conclusion, the team's hypothesis was correct. Although having the smallest height proved to be true, the smallest length and width didn't result in the smallest C_d. From this point forward the sizes of 108L, 22W, and 37H will be used to create a fairing that will be modified in multiple aspects, thus leading to a printed model for physical testing.

3.4 STEERING

There are several key steering geometries for a two front-wheeled Trike. These include: a caster, camber, kingpin and axle offset. For this system a custom knuckle will be made, which will pivot in a tube and be connected to the frame using a standard 1-1/8 headset. This is the part on a typical bicycle that attaches the fork to the frame and allows it to pivot using a pair of bearings. The knuckle can be seen in Figure 13 and, combined with the frame, incorporates all of the steering geometries.

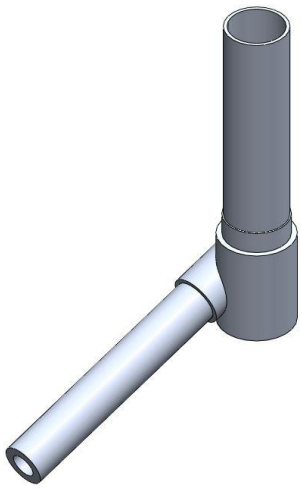

Figure 13- Steering Knuckle

The first steering geometry is the caster angle. Caster is the degree of the pivot angle tilted forward, as shown in Figure 14 below. The caster angle is critical because it causes the wheels to automatically return to a straight position after turning. This geometry is not exclusive to human powered vehicles, and is used in almost all vehicles with two front steering wheels. Most automobiles use a 4-5 degree caster angle while go carts and racing vehicles generally use a much more aggressive angle [4]. The team selected to use, roughly, a 13 degree caster angle due to research and past experience. Horwitz used a 12 degree angle and an old NAU HPVC bike used a 12.5 degree angle and handled extremely well [4].

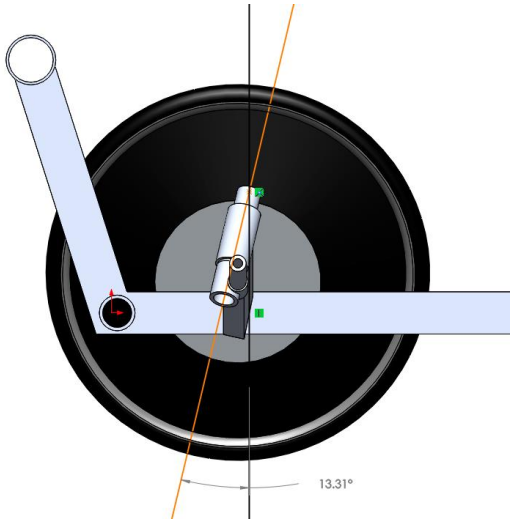

Figure 14- Caster Angle

The next important steering angle is the camber. This is the angle from the wheels to vertical, which can be seen in Figure 15. If the tops of the wheels are closer than the bottoms, the vehicle is said to have negative camber. If the bottoms of the wheels are closer, then the vehicle has a positive camber. Most vehicles have a negative or neutral camber [4]. The team decided to go with a 12 degree negative camber for several reasons. These reasons include improved stability and loading on the wheels. Bicycle wheels are designed to be loaded vertically because the loading stays vertical in relation to the wheel, while a typical bicycle leans into a turn. This application, however, will have very high side loading on the wheels. Therefore, having a drastic negative camber helps keep more of the force in the vertical axis of the wheel. Another reason is past experience with similar caster angle.

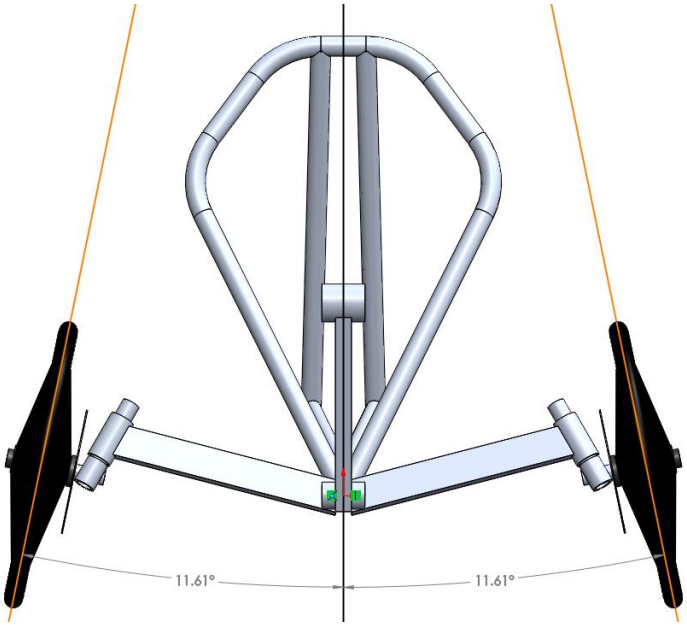

Figure 15- Camber Angle

The next geometry is the kingpin angle. This is the angle of the pivot axis from vertical viewing from the front as can be seen in Figure 16 below. Some vehicles implement center point steering, in which the tire pivots about the tire patch, where the tire contacts the ground. Center point steering is desirable because it allows for more precise and efficient steering [4]. The efficiency comes from helping eliminate tire scrubbing, which is unnecessary friction when the tires turn. With the geometry given, the kingpin angle becomes 30 degrees to achieve center point turning.

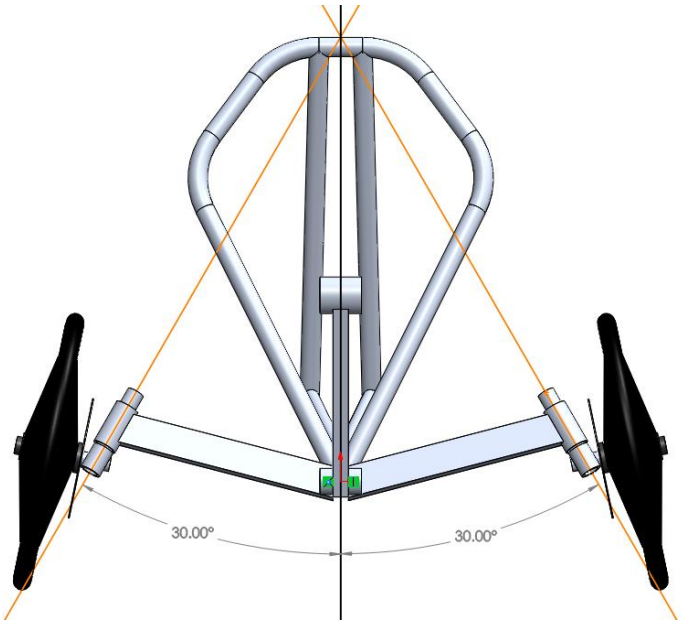

Figure 16- Kingpin Angle

The final critical geometry is the axle offset. This offset helps drastically with steering stability. If the axle of the wheel is in front of or in line with the pivot axis, the caster angle is negated. This can also cause undesirable steering motions. The most stable position is for the axle to be behind the pivot axis [4]. The team has chosen to put the axle 0.5 inches behind the pivot axis because of research and past experience with old NAU HPVC vehicles.

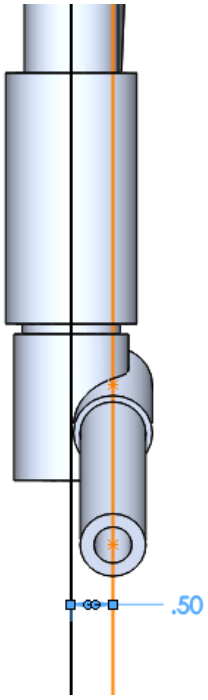

Figure 17- Axle Offset

After determining all of the geometries for steering, the final outside dimensions of the steering knuckle were finalized. Weight is a large factor for this vehicle and the knuckles are an easy part to optimize to try and reduce weight. The knuckles used in past NAU HPVC vehicles have both been steel and aluminum. Analysis was done using different configurations of aluminum and steel. The FEA testing analysis was set up with two fixture points, one at the top and one at the bottom, to simulate the two bearings in the headset. A distributed force was then applied to the axle to simulate the force that would be on the axle with the wheel; this can be seen in Figure 18 below. This force was determined using accelerometer data, as shown in Appendix A. The force was then multiplied by a factor to account for issues with the test as well as accelerometer location.

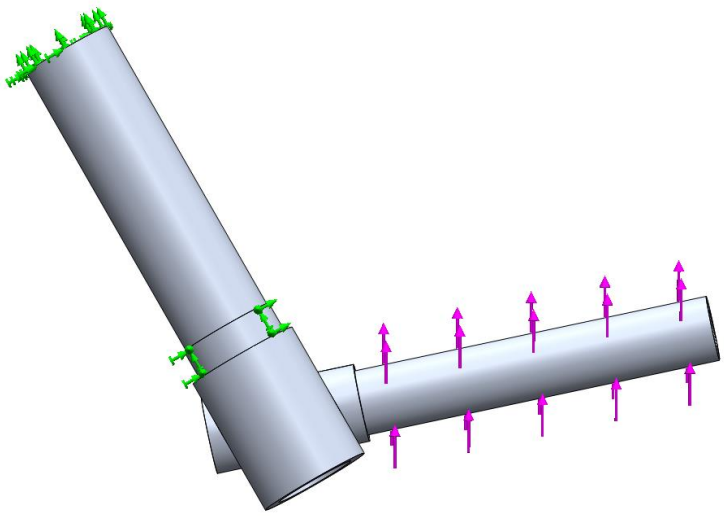

Figure 18- FEA Setup

The first configuration tested was 6061T6 heat treated aluminum, seen in Figure 19. Both the steer tube and axle are hollow and are somewhat thin-walled. The force applied was 353 lbf. The yield strength of the aluminum is 40,000 psi and a max stress of 20,000 psi resulted in a factor of safety of 2 before yield. The weight of this configuration is 0.43 lbs.

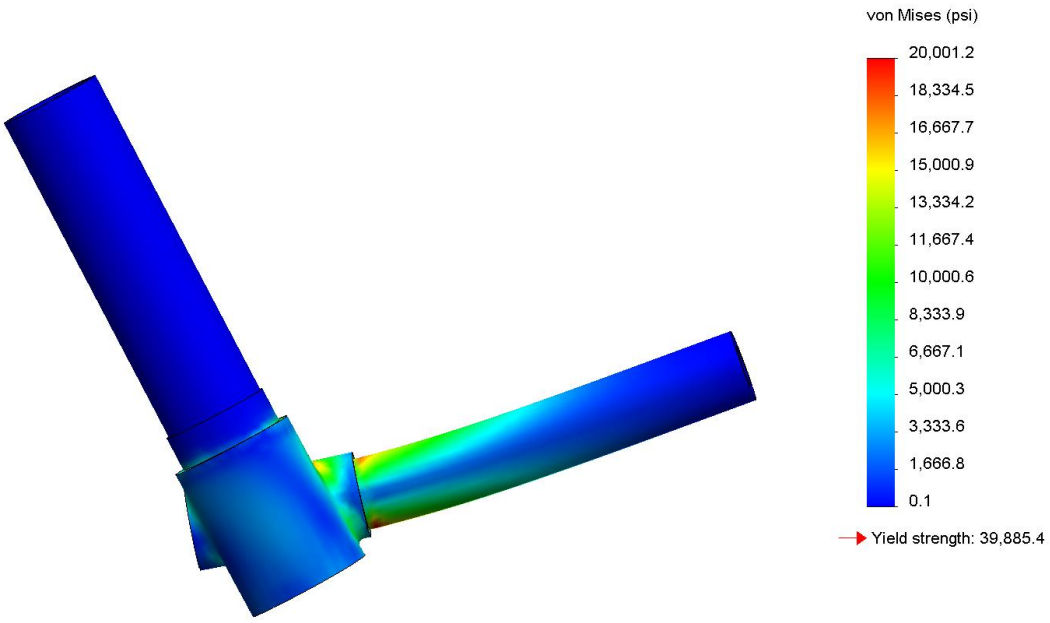

Figure 19- Aluminum FEA

The next configuration is 4130 chromoly, seen in Figure 20. This configuration was optimized to make the tubes as thin as possible while minimizing stresses. The force and fixtures applied were the same as the previous configuration. The outside dimensions of this setup are

also identical to the previous configuration. Only the inside diameters changed to reduce material and weight. The yield strength of the chromoly is 67,000 psi and a max stress calculated was 34,000 psi, leaving the factor of safety at 2 for yielding. The weight of this setup is 0.73 lbs, despite having the same factor of safety as the aluminum.

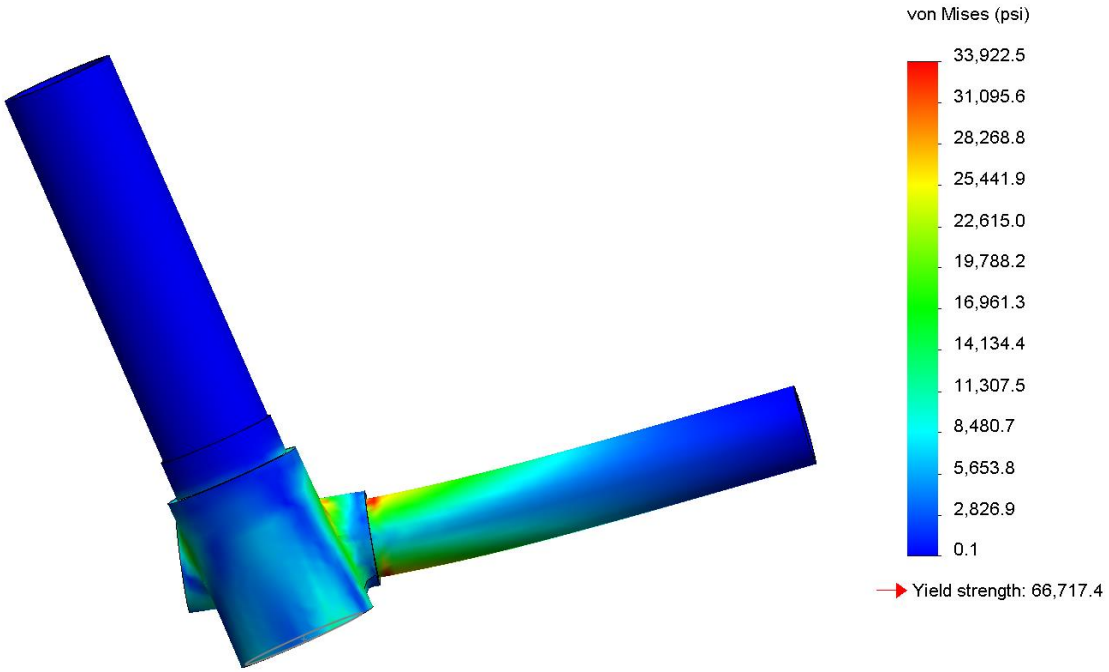

Figure 20- Chromoly FEA

3.5 DRIVETRIAN

To analyze the drivetrain of the vehicle a MATLAB code was used to select the optimal gear ratios to achieve a maximum velocity with minimal rider effort. These two aspects of the drivetrain were analyzed as the project had a client given requirement of reaching a speed of 40 mph as well as a competition based requirement of navigating a course with sections of high and low speeds.

To begin the analysis an average and maximum rider cadence was found from a rider position study. The results of the rider position study for average power can be seen in Figure 12 in the ergonomics analysis section. From this rider position study the instantaneous maximum and average cadences were collected and can be displayed in Table 4 below.

Table 4- Rider Cadence

	Average Cadence (RPM)	Max Cadence (RPM)
Rider 1	70	149
Rider 2	101	133
Rider 3	91	149
Rider 4	93	141
Rider 5	91	135
Rider 6	90	143
Average	**89.33**	**141.67**
Rounded Average	**90**	**140**

The results presented in the table allowed the team to select two cadence values to be used in analysis. These included an average cadence of 90 rpm for extended periods of time and a maximum cadence of 110 rpm when a top speed is desired. The value of 110 rpm was selected by viewing the maximum instantaneous cadences displayed in the table, 140 rpm, and selecting a cadence that was 20% lower than the lowest achieved maximum in order to better represent an achievable maximum.

After establishing the two rider cadences to be analyzed, the team used a MATLAB code to calculate the gear ratios and respective speeds for the vehicle. In order to achieve the client requirement of reaching 40 mph the team chose to select a gear ratio that provided a max speed 5% over the requirement, a maximum speed of 42.25 mph. The vehicle needed to reach this speed while attaining the lowest gear ratio on the easiest gears. Table 5 below displays the gear ratio and speed at each of the positions on the rear cassette.

Table 5– Gear Ratios and Speeds

Gear Ratio	Speed at 90 RPM (MPH)	Speed at 110 RPM (MPH)
1.50	10.56	12.91
1.69	11.88	14.52
1.93	13.58	16.60
2.25	15.84	19.36
2.57	18.11	22.13
3.00	21.13	25.82
3.38	23.77	29.05
3.86	27.16	33.20
4.50	31.69	38.73
4.91	34.57	**42.25**

As seen in the table, the vehicle has a gear ratio of reaching 42.25 mph while having a gear ratio of 1.5 in the lowest possible gear. By selecting a configuration with a low gear ratio the vehicle will be capable of the start and stop motion on the course as well as reaching a max speed.

3.6 INNOVATION

The team intends to design a vehicle that is operable in a range of climate conditions. Of upmost concern was comfort of the rider in warm conditions. Even mildly warm ambient air temperatures can make the interior vehicle a harsh environment for physical activity. With this in mind, the team is designing a method for circulating ambient air through the shell during operation in typical weather. This system will be passive, lightweight, and removable to condition the incoming air in more adverse environments.

The first design placed a cold, finned block in line with incoming circulation air, with the intention that it would remove energy, thus cooling the air before it flows over the operator. The block itself would be machined out of aluminum, with a sealed hollow cavity filled with water. An ice core would allow the block to remain cold for longer periods of time. As the ice undergoes phase transition to water, the fin base temperature will remain semi constant. The large amount of energy required to force the phase transition, as represented by the Heat of Fusion, will allow for more energy absorption. A vehicle owner would place the finned block in their freezer for an adequate amount of time prior to driving the vehicle, at which time, the block would be mounted in its location inside the vehicle shell. As warm air passes over the fins, its energy is transferred to the aluminum fins and ice core, eventually melting the internal ice and raising it to ambient temperature. A concept model of this system can be seen in Figure 21, with the blue mass representing the cold block.

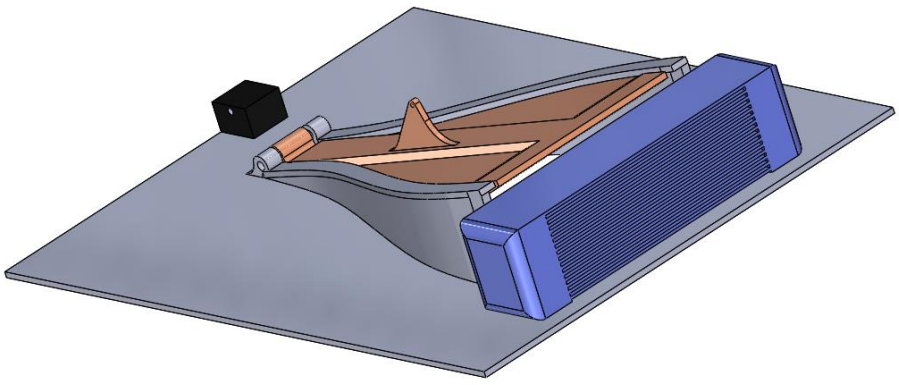

Figure 21– Innovation

With internal vehicle dimensions unavailable, a generous model was developed to represent a plausible outcome for finned surface area with favorable material properties. An assumption of 6 fins with .1m by .05 m dimensions was made, with their thickness small enough to be negligible. The thermal resistance of the aluminum block shell was also assumed negligible, effectively modeling the fins and base as made from ice itself. A convection coefficient, h, was calculated using from Equation 10 for mixed boundary layer conditions.

$$\bar{h_l} = \frac{\overline{Nu}_l k}{l} \tag{10}$$

where

$$\overline{Nu}_l = \left(.037 Re_l^{\frac{4}{5}} - A \right) Pr^{\frac{1}{3}} \tag{11}$$

And

$$A = .037 Re_{l,c}^{4/5} - .664 Re_{l,c}^{1/2} \tag{12}$$

Equations 10, 11, and 12 result in a convection coefficient of 31 $\frac{w}{m^2 \cdot k}$ at a velocity off 9 m/s (20 mph). Assuming an ambient air temperature, a surface area, and a flow rate of 26°C, .0625 m^2, and 9 m/s respectively, the ice will remain within 12° of its initial temperature for roughly 46 minutes. 46 minutes is a sufficient period of time for a cooling system to operate, however this design is limited by quality of performance rather than longevity of performance. The system is limited by its small size and weight constraints which simply do not allow for amount of surface area required to produce the desired cooling of incoming air. With the current assumptions, only a 1°C temperature drop is achieved.

The team plans to explore methods to increase the surface area exposed to incoming airflow as well as evaluate the efficacy of a small scale evaporative cooling mechanism that would replace the finned cold block concept.

The air for system will enter the vehicle interior through a servo operated, closable duct embedded into the composite fairing. This duct is operated by the vehicle rider through the use of a button in the cockpit. The ability to close the duct serves two purposes. First, as daytime high temperatures drop, the rider may find that they wish for a warmer environment to travel in. Closing the duct will reduce air circulation and begin to increase the interior temperature as the rider's body puts out heat. Secondly, these ducts will introduce a measureable amount of aerodynamic drag on the vehicle; the ability to seal off this port will give the rider the option to temporarily sacrifice internal temperature for a higher vehicle velocity.

As previously stated, this duct will be actuated by a servo with 180° of operating range. The linkage that transfers rotation from the servo to the duct flap is designed so that lockout occurs at the extremes of the flap position, requiring a minimal amount of batter power to hold the flap in any one location. This is achieved with the usage of an 8:1 lever arm ratio. This part will be fabricated using a fused deposition modeling additive manufacturing process.

Lighting systems are the competition standard for roadway communication. Brake lights, tail lights, headlights, and turn signals are required for maximum competition ranking. However, the quality and visibility of such lights is not regulated.

After evaluating the visibility of lights of automobiles the team found it necessary for any light on a vehicle to be visible from a minimum of 180° horizontally. This requirement is flexible in that it allows either the hardware of the light itself to be visible or a clear, unquestionable view of the light emitted by the hardware.

It was also determined that successful turn signals must be visible from behind, to the side, and in front of the vehicle. Rather than placing two turn signal light sets on the human powered vehicle like those of an automobile, the team will include a continuous LED strip around the circumference of the front wheel fairings. The arrangement of the light safety and communication systems and their ranges of visibility can be seen in Figure 22.

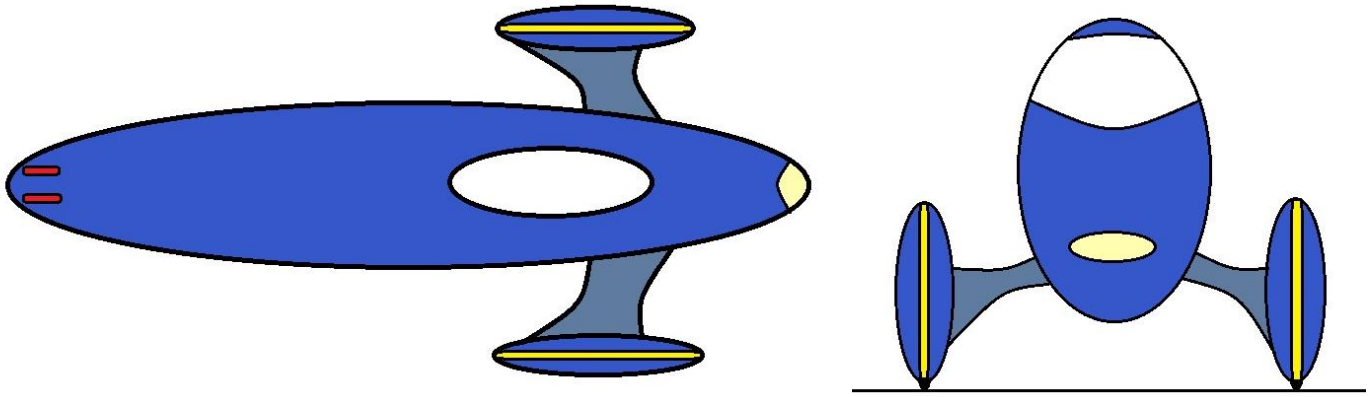

Figure 22- Vehicle Lighting Arrangement

The team wanted to ensure that the vehicle would resist roll over during aggressive driving. To accomplish this, the width of the vehicle was designed so that the tires would lose traction before the vehicle initiated a tip.

Analysis was performed to determine the minimum front wheel width that would avoid tipping conditions. First a total vehicle and rider weight of 240lbs was assumed to be distributed evenly over all three wheels during static scenarios. However, for tipping conditions to occur, all

the system's mass would be carried by the rear and one front wheel. This creates a new distribution of 80lbs per tire in contact with the ground. The static friction coefficient, μ_s, of rubber on asphalt was assumed to be 0.8. The total system center of gravity was assumed at the mid plane of the vehicle, 50% of the way between the front and back wheels, and 14in above the ground.

For tipping to occur during an aggressive turn, the lateral inertial force, F, acting at the center of gravity must be so great that the moment it creates about the tire contact patches must be greater than the moment created by the vehicle weight W about the same contact patch. However, the lateral inertial force F must also be lower in magnitude than the maximum frictional force, f, before movement begins, where

$$f = \mu_s N \tag{13}$$

Or in this case

$$f = 0.8 * 120lbs = 96lbs \tag{14}$$

Finally, slipping at both wheels in contact with the ground is not required to avoid a tip. One wheel breaking loose will cause a shift in the vehicle's direction of travel and weight distribution to adequately avoid a tip.

If slipping is to occur before tipping, the lateral inertial force F required to overcome the weight of the vehicle must be significantly greater than the maximum frictional force f at either of the two tires carrying the load of the vehicle. See Figure 23 for a diagram of the force relationship.

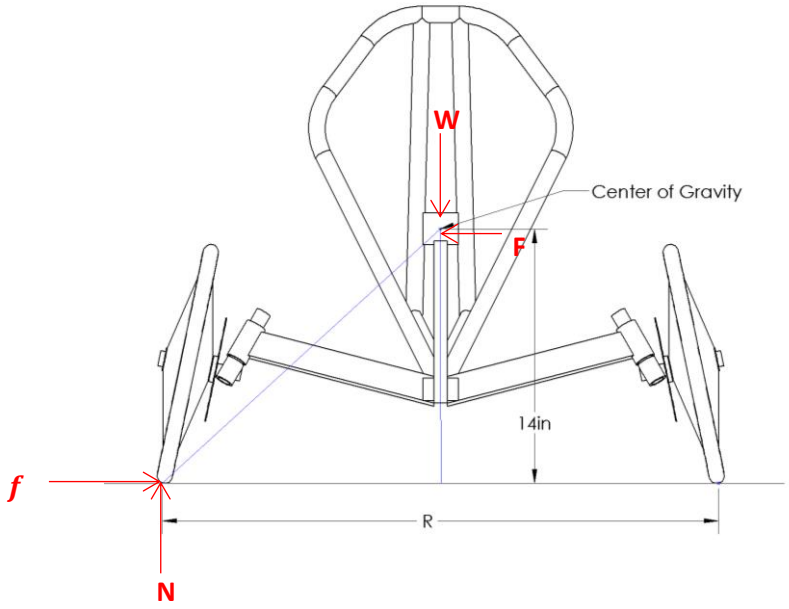

Figure 23- Tipping Analysis FBD

For a three wheeled vehicle, lateral tipping occurs about an axis drawn from the contact patch of either of the two front wheels to the contact patch of the rear wheel, also shown in Figure 24. Because of this, the distance A from the center of gravity to the tipping axis is not simply half the vehicle width. Instead, the distance to the tipping axis can be defined by the geometry in Figure 24.

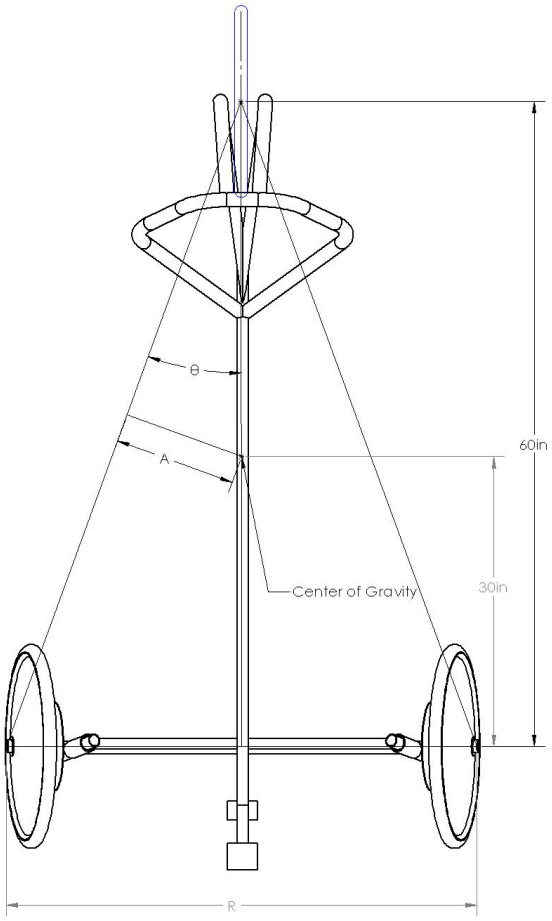

Figure 24- Tipping Axis Location

Solving for the minimum required distance A to avoid tipping requires setting $F \Rightarrow f$ and can be seen below:

$$W * A = F * 14in \tag{15}$$

Substituting in the assumptions and solving for A gives

$$A \geq 5.6in \tag{16}$$

Back solving for the minimum front wheel width R gives

$$\theta = \sin^{-1}\frac{5.6}{30} = 10.76° \quad (17)$$

$$R = 2L\tan\theta = 23in \quad (18)$$

23in was determined to be the minimum critical width to avoid tipping during aggressive turning. However, bicycle lanes are usually a minimum of 48inches in width. Subsequently, the width of the vehicle front wheels was chosen to be 42in, which will allow for a stable vehicle on all types of terrain, yet still capable of traveling within bicycle specific lanes with space on either side.

ASME continually pushes entrants to be innovative in the design and manufacturing of their vehicles. Human powered vehicles are often one-off mobiles fabricated from exotic, costly materials, especially when their main purpose is to be used as a competition entry. It was felt that an effective way to offset these costs yet still have a vehicle that performs competitively was to seek out alternative, recycled materials. More specifically, we will attempt to recycle scrap materials from our own manufacturing of the vehicle. Tables 6 and 7 show a list of waste materials traditionally produced during the fabrication of a human powered vehicle. Combinations of these materials will be attempted, with the desire of creating a composite material with properties that can be utilized on the vehicle. Currently the team is continuing to collect these materials.

Table 6- Possible Recyclable Reinforcement Materials

Reinforcement Materials	Source
Aluminum chips as collected or powered	Machining of components
Wood Fibers	Fixtures and shipping
Powdered previously laid up carbon fiber	Last year's vehicle, research projects
Cardboard	Shipping supplies
Scrap carbon fiber and fiberglass clippings	Local composite product manufactures

Table 7- Possible Recyclable Matrix Materials

Matrix Materials	Source
Epoxy Resin	Left over from previous and current builds
High density polyethlyne	Discarded water bottles and shipping materials
Nylon	Dupont material samples
Derlin	Dupont material samples
ABS	Contaminated FDM materials

4.0 PROJECT SCHEDULE

The team is currently on schedule to complete the design and analysis portion of the project by the 2013 winter break. In addition to the design and analysis phase, the team is also ahead of schedule on the process of prototyping and ordering needed materials. The team will work to stay on track based on the Gantt chart through the competition in May 2014. The Gantt chart can be found in Appendix B, and displays the current progress on each task listed.

5.0 CONCLUSION

Team 9 has completed a series of analysis tasks in order to determine the best results for each subsection of the vehicle. Each analysis task assisted in material selection, component design, and vehicle configuration. Through the use of these numerical and analytical results, the team was able to design an optimized vehicle.

As the frame of the vehicle is one of the core components, it was broken into three separate components. These included the center tube, the outriggers, and the rollover protection system. Through the analysis, the center tube and out riggers were will be made out of 1.5”X1.5” aluminum square tubing. This will allow minimal torsional and lateral deflection while keeping weight to a minimum. After completing finite element analysis, the roll bar protection system proved to meet the ASME challenge requirements. The team conducted a series of experiments to determine the ideal rider position. This rider study proved that an ideal angle of 122° would provide the best average power while providing adequate visibility. Using the 122° rider position a fairing size was optimized for the lowest coefficient of drag. This resulted in a faring of roughly 108” in length, width of 22” and a height of 37”, with a coefficient of drag of 0.025. To analyze the vehicles steering, four dimensions were evaluated: caster, camber, kingpin, and axle offset. These results were a 13° caster angle, 12° camber angle, 30° kingpin angle and 0.5 in angle offset. In addition to the steering geometry, the steering knuckle was analyzed using finite element analysis. This proved that the knuckles should be made from aluminum and will have a factor of safety of 2. Using the data collected from the rider position study the vehicles drivetrain was analyzed to determine the optimal gear ratio while reaching a max speed above 40 mph. To meet the competitions innovation requirements the team investigated a finned cold block cooling system, safety systems and sustainable manufacturing. To analyze vehicle safety a lighting system was evaluated and a tipping analysis was computed to find the vehicles width of 42in. Lastly, the use of recycled materials was investigated to find potential materials for future testing. Through all of the analysis completed, the team is on their way to building a vehicle capable of meeting all requirements and goals set forth by the client and competition.

6.0 REFERENCES

[1] R.C. Hibbeler, *Structural Analysis*, New Jersey, Pearson Prentice Hall, 2012

[2] R. G. Budynas and J. K. Nisbett, *Shigley's Mechanical Engineering Design,* New York, McGraw-Hill, 2011

[3] Philip J. Pritchard and John C. Leylegian, *Introduction to Fluid Mechanics*, Manhattan College: John Wiley & Sons, Inc., 2011.

[4] R. Horwitz. (2010). The Recumbent Trike Design Primer (8.0) [Online]. Available: http://hellbentcycles.com/trike_projects/Recumbent%20Trike%20Design%20Primer.pdf

[5] R.C. Hibbeler, *Engineering Mechanics – Statics*, Pearson Prentice Hall, 2010

7.0 APPENDIX

APPENDIX A– Accelerometer Data

- Test 1 is a run at low speed towards two .75inch tall wood slats - accelerometers on rear axle the maximum applied force for test 1 is 222.5 LBS
- Test 2 is a run at high speed towards two .75inch tall wood slats - accelerometers on rear axle the maximum applied force for test 2 is 243.8 LBS
- Test 3 is a run at high speed towards two .75inch tall wood slats - accelerometers on front axle the maximum applied force for test 3 is 271.8 LBS
- Test 4 is a run at high speed towards two .75inch tall wood slats - accelerometers on mid belly of bike the maximum applied force for test 4 is 182.6 LBS

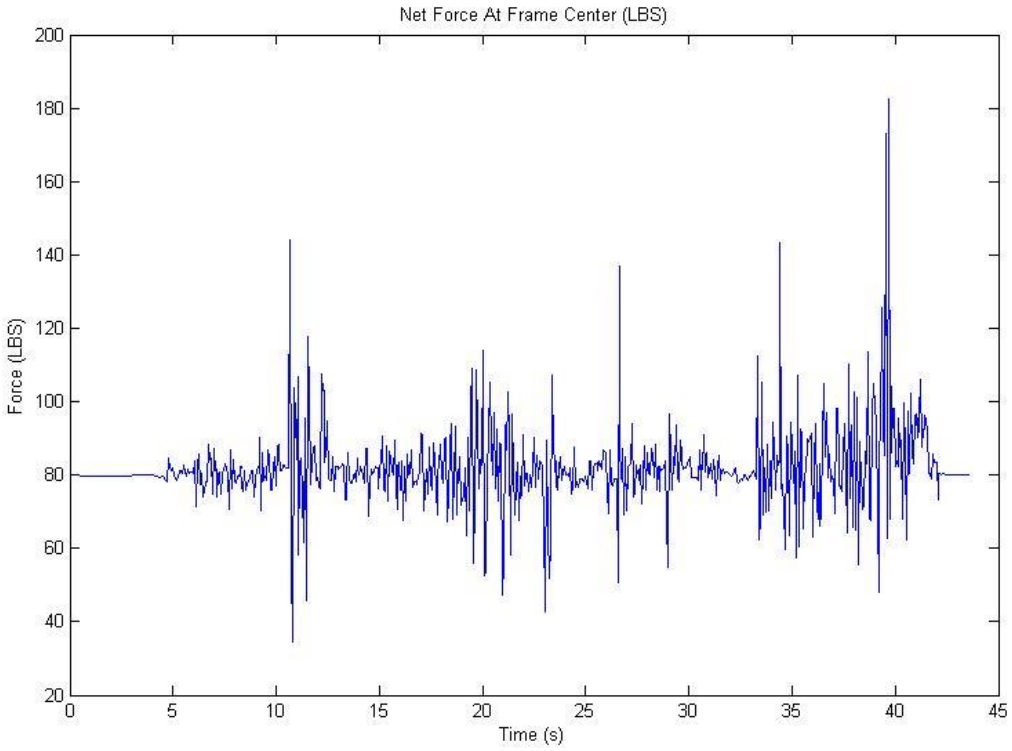

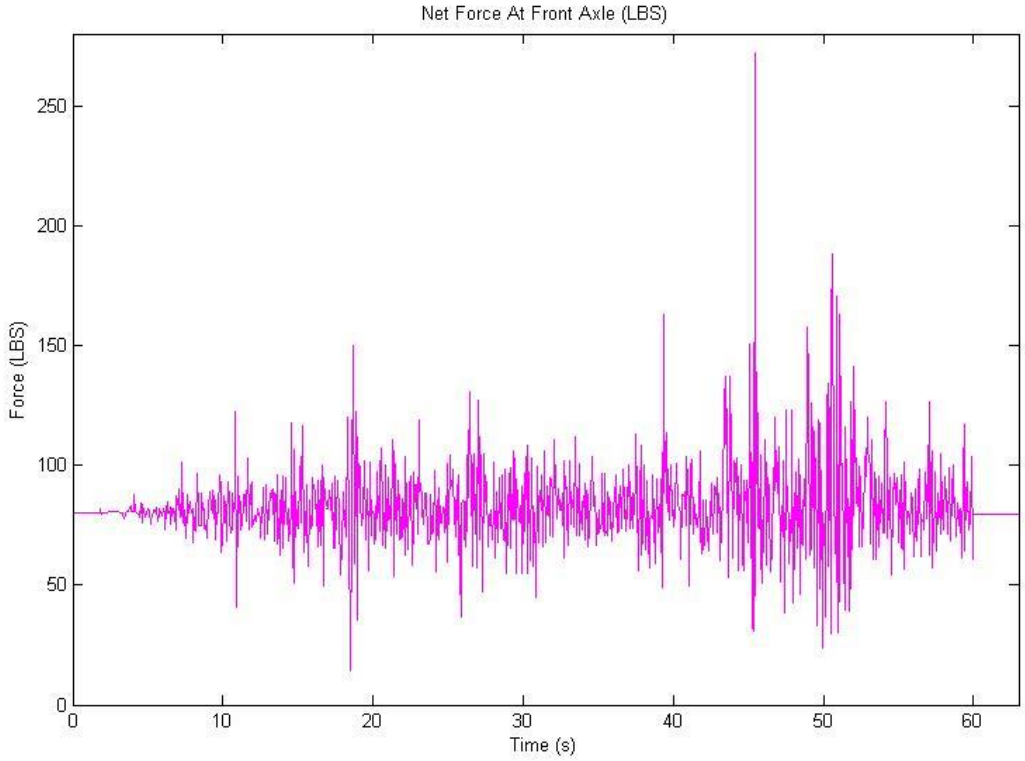
Net Force At Front Axle (LBS)
Force (LBS)
Time (s)
0
50
100
150
200
250
0
10
20
30
40
50
60

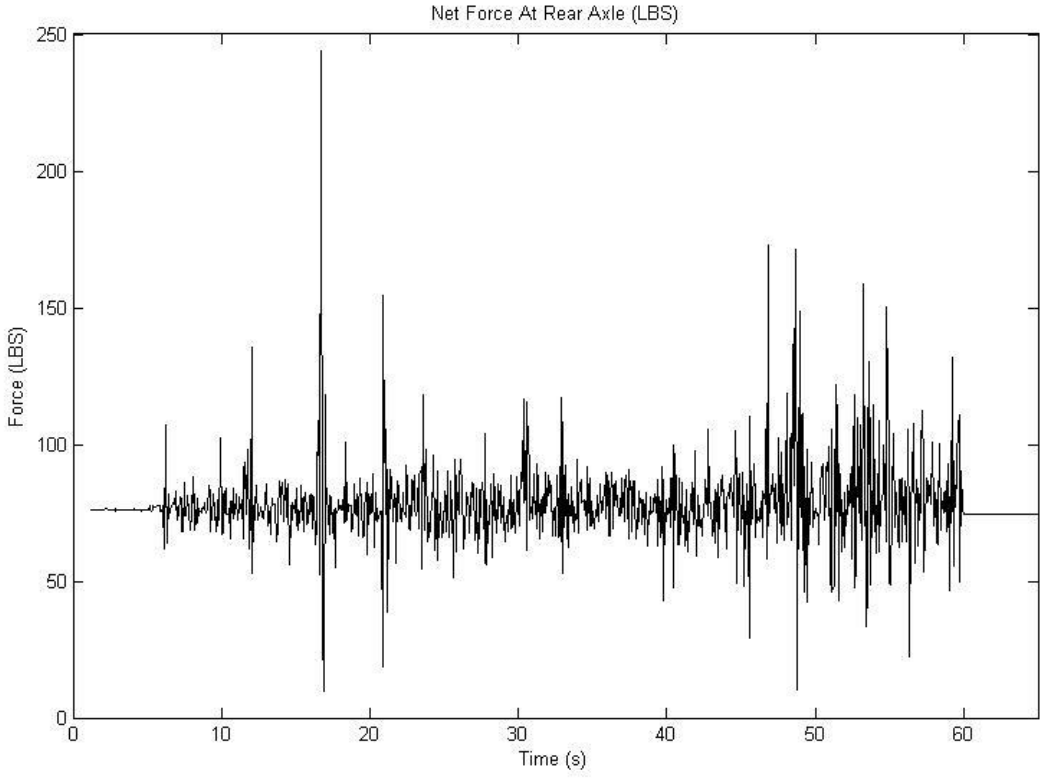
Net Force At Rear Axle (LBS)
Force (LBS)
Time (s)
0
50
100
150
200
250
0
10
20
30
40
50
60

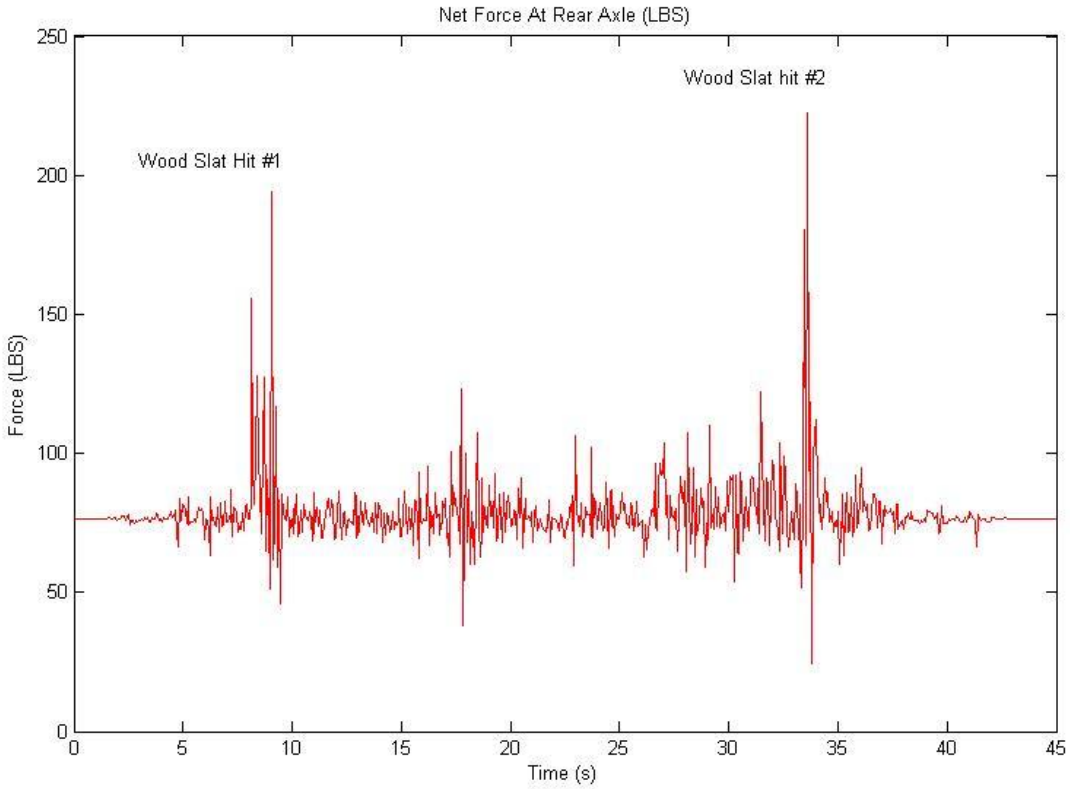
Net Force At Rear Axle (LBS)
Wood Slat hit #2
Wood Slat Hit #1
Force (LBS)
Time (s)
250
200
150
100
50
0
0
5
10
15
20
25
30
35
40
45

APPENDIX B– Gantt Chart

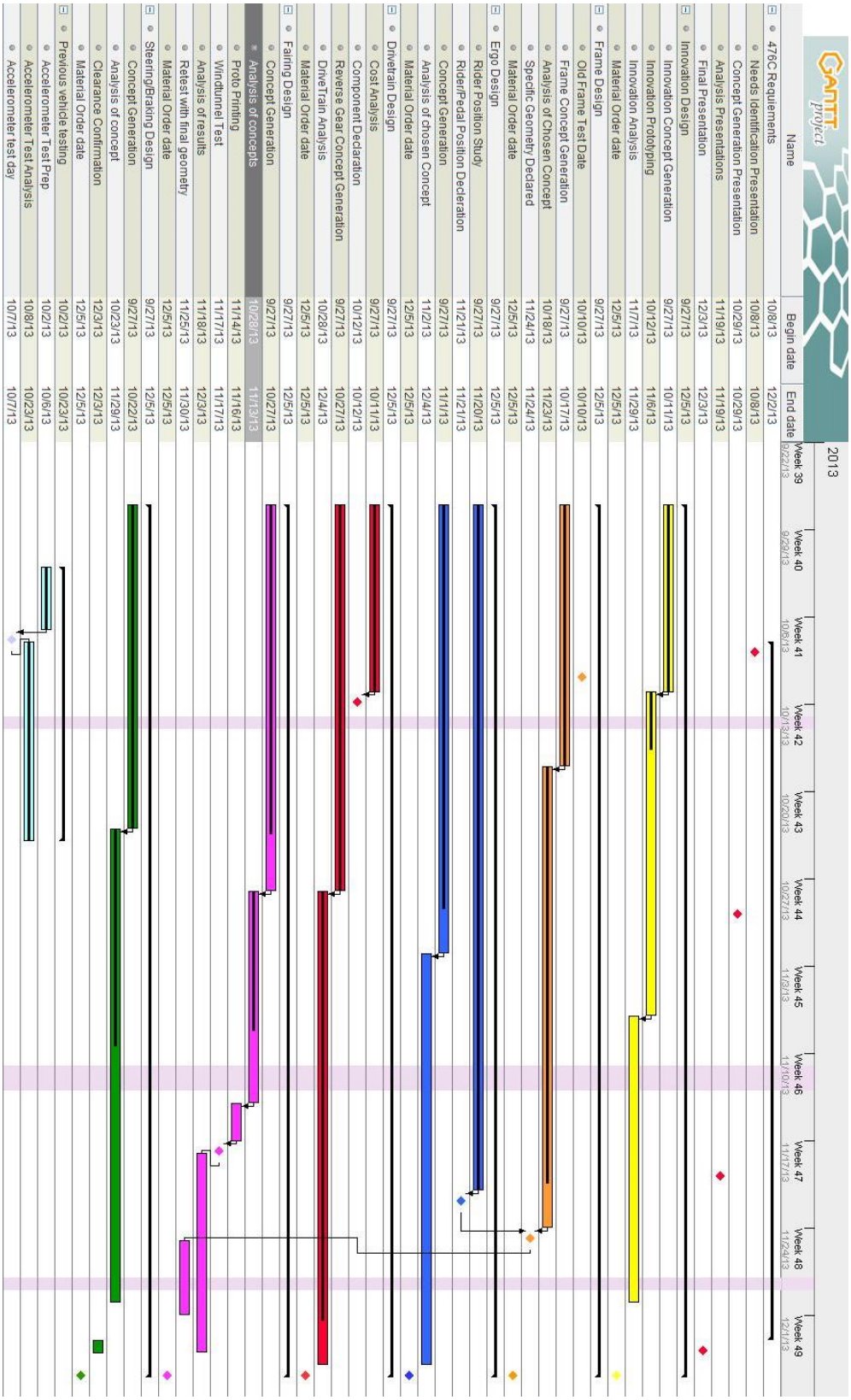

APPENDIX C– Coefficient of Drag Results

Table 8- Change in Length

Length (in)	Width (in)	Height (in)	Speed (in/s)	Force (lbf)	Area (in^2)	C_d
96	18	33	704	0.4572	595.12	0.033
102	18	33	704	0.3775	579.41	0.028
108	18	33	704	0.3897	576.73	0.029
96	18	37	704	0.5995	681.54	0.038
102	18	37	704	0.4110	670.37	0.026
108	18	37	704	0.5400	670.51	0.035
96	18	39	704	0.6008	727.01	0.036
102	18	39	704	0.4123	751.53	0.024
108	18	39	704	0.5919	718.78	0.036
96	20	33	704	0.3215	624.85	0.022
102	20	33	704	0.3020	611.54	0.021
108	20	33	704	0.3198	600.8	0.023
96	20	37	704	0.5132	716.58	0.031
102	20	37	704	0.4957	702.1	0.030
108	20	37	704	0.4895	701.49	0.030
96	20	39	704	0.5913	763.3	0.033
102	20	39	704	0.5336	755.25	0.030
108	20	39	704	0.5085	750.21	0.029
96	22	33	704	0.3878	662.26	0.025
102	22	33	704	0.4633	651.16	0.031
108	22	33	704	0.3926	633.91	0.027
96	22	37	704	0.5417	760.07	0.031
102	22	37	704	0.5659	753.55	0.032
108	22	37	704	0.4376	740.06	0.025
96	22	39	704	0.6102	809.7	0.032
102	22	39	704	0.5902	805.48	0.032
108	22	39	704	0.4914	792.63	0.027
96	24	33	704	0.4520	700.15	0.028
102	24	33	704	0.3914	683.3	0.025
108	24	33	704	0.3361	678.4	0.021
96	24	37	704	0.6170	803.72	0.033
102	24	37	704	0.5126	790.64	0.028
108	24	37	704	0.5767	788.48	0.032
96	24	39	704	0.7177	855.92	0.036
102	24	39	704	0.5843	844.81	0.030
108	24	39	704	0.5251	845.19	0.027

Table 9- Change in Width

Length (in)	Width (in)	Height (in)	Speed (in/s)	Force (lbf)	Area (in^2)	C_d
96	18	33	704	0.4572	595.12	0.033
96	20	33	704	0.3215	624.85	0.022
96	22	33	704	0.3878	662.26	0.025
96	24	33	704	0.4520	700.15	0.028
96	18	37	704	0.5995	681.54	0.038
96	20	37	704	0.5132	716.58	0.031
96	22	37	704	0.5417	760.07	0.031
96	24	37	704	0.6170	803.72	0.033
96	18	39	704	0.6008	727.01	0.036
96	20	39	704	0.5913	763.3	0.033
96	22	39	704	0.6102	809.7	0.032
96	24	39	704	0.7177	855.92	0.036
102	18	33	704	0.3775	579.41	0.028
102	20	33	704	0.3020	611.54	0.021
102	22	33	704	0.4633	651.16	0.031
102	24	33	704	0.3914	683.3	0.025
102	18	37	704	0.4110	670.37	0.026
102	20	37	704	0.4957	702.1	0.030
102	22	37	704	0.5659	753.55	0.032
102	24	37	704	0.5126	790.64	0.028
102	18	39	704	0.4123	751.53	0.024
102	20	39	704	0.5336	755.25	0.030
102	22	39	704	0.5902	805.48	0.032
102	24	39	704	0.5843	844.81	0.030
108	18	33	704	0.3897	576.73	0.029
108	20	33	704	0.3198	600.8	0.023
108	22	33	704	0.3926	633.91	0.027
108	24	33	704	0.3361	678.4	0.021
108	18	37	704	0.5400	670.51	0.035
108	20	37	704	0.4895	701.49	0.030
108	22	37	704	0.4376	740.06	0.025
108	24	37	704	0.5767	788.48	0.032
108	18	39	704	0.5919	718.78	0.036
108	20	39	704	0.5085	750.21	0.029
108	22	39	704	0.4914	792.63	0.027
108	24	39	704	0.5251	845.19	0.027

Table 10- Change in Height

Length (in)	Width (in)	Height (in)	Speed (in/s)	Force (lbf)	Area (in^2)	C_d
96	18	33	704	0.4572	595.12	0.033
96	18	37	704	0.5995	681.54	0.038
96	18	39	704	0.6008	727.01	0.036
96	20	33	704	0.3215	624.85	0.022
96	20	37	704	0.5132	716.58	0.031
96	20	39	704	0.5913	763.3	0.033
96	22	33	704	0.3878	662.26	0.025
96	22	37	704	0.5417	760.07	0.031
96	22	39	704	0.6102	809.7	0.032
96	24	33	704	0.4520	700.15	0.028
96	24	37	704	0.6170	803.72	0.033
96	24	39	704	0.7177	855.92	0.036
102	18	33	704	0.3775	579.41	0.028
102	18	37	704	0.4110	670.37	0.026
102	18	39	704	0.4123	751.53	0.024
102	20	33	704	0.3020	611.54	0.021
102	20	37	704	0.4957	702.1	0.030
102	20	39	704	0.5336	755.25	0.030
102	22	33	704	0.4633	651.16	0.031
102	22	37	704	0.5659	753.55	0.032
102	22	39	704	0.5902	805.48	0.032
102	24	33	704	0.3914	683.3	0.025
102	24	37	704	0.5126	790.64	0.028
102	24	39	704	0.5843	844.81	0.030
108	18	33	704	0.3897	576.73	0.029
108	18	37	704	0.5400	670.51	0.035
108	18	39	704	0.5919	718.78	0.036
108	20	33	704	0.3198	600.8	0.023
108	20	37	704	0.4895	701.49	0.030
108	20	39	704	0.5085	750.21	0.029
108	22	33	704	0.3926	633.91	0.027
108	22	37	704	0.4376	740.06	0.025
108	22	39	704	0.4914	792.63	0.027
108	24	33	704	0.3361	678.4	0.021
108	24	37	704	0.5767	788.48	0.032
108	24	39	704	0.5251	845.19	0.027

APPENDIX D– Rider Position Study Data

3 Minute Test at 130°							
	Average Power (W)	Max Power (W)	Average Heart Rate (BPM)	Average Cadence (RPM)	Energy Expended (Kj)	Rider Weight (Kg)	Power To Weight
Alex	195	312	177	68	35	83.9	2.32
Erik	251	439	164	97	47	70.3	3.57
Heather	172	301	164	80	32	58.96	2.92
Phillip	140	521	160	87	27	86.2	1.62
Kevin	245	443	166	94	44	83.9	2.92
Matt	175	311	163	85	33	63.5	2.76

3 Minute Test at 122°							
	Average Power (W)	Max Power (W)	Average Heart Rate (BPM)	Average Cadence (RPM)	Energy Expended (Kj)	Rider Weight (Kg)	Power To Weight
Alex	229	492	189	70	42	83.9	2.73
Erik	307	426	174	101	55	70.3	4.37
Heather	154	491	170	91	28	58.96	2.61
Phillip	159	382	164	93	29	86.2	1.84
Kevin	242	406	175	91	47	83.9	2.88
Matt	174	230	158	90	31	63.5	2.74

3 Minute test at 115°							
	Average Power (W)	Max Power (W)	Average Heart Rate (BPM)	Average Cadence (RPM)	Energy Expended (Kj)	Rider Weight (Kg)	Power To Weight
Alex	194	361	183	69	35	83.9	2.31
Erik	287	381	165	95	53	70.3	4.08
Heather	131	503	169	84	25	58.96	2.22
Phillip	131	427	164	89	25	86.2	1.52
Kevin	244	422	175	98	45	83.9	2.91
Matt	188	319	139	93	34	63.5	2.96

Max Test at 130°								
	Average Power (W)	Max Power (W)	Average Heart Rate (BPM)	Average Cadence (RPM)	Max Cadence (RPM)	Energy Expended (Kj)	Rider Weight (Kg)	Power To Weight
Alex	421	1130	177	95	155	25	83.9	13.47
Erik	351	928		94	131	16	70.3	13.20
Heather	188	442	148	61	86	12	58.96	7.50
Phillip	318	865	171	99	145	21	86.2	10.03
Kevin	335	762	159	98	140	20	83.9	9.08
Matt	310	953	158	97	142	20	63.5	15.01

Max Test at 122°								
	Average Power (W)	Max Power (W)	Average Heart Rate (BPM)	Average Cadence (RPM)	Max Cadence (RPM)	Energy Expended (Kj)	Rider Weight (Kg)	Power To Weight
Alex	377	1012	172	94	149	24	83.9	12.06
Erik	323	948	158	85	133	21	70.3	13.49
Heather	223	568		87	149	14	58.96	9.63
Phillip	387	779	170	90	141	21	86.2	9.04
Kevin	351	688	171	106	135	23	83.9	8.20
Matt	290	736	155	101	143	20	63.5	11.59

Max test at 115°								
	Average Power (W)	Max Power (W)	Average Heart Rate (BPM)	Average Cadence (RPM)	Max Cadence (RPM)	Energy Expended (Kj)	Rider Weight (Kg)	Power To Weight
Alex	425	1174		89	155	25	83.9	13.99
Erik	273	945	150	89	149	17	70.3	13.44
Heather	188	510	151	91	132	12	58.96	8.65
Phillip	337	855	176	93	130	23	86.2	9.92
Kevin	338	585	173	103	146	21	83.9	6.97
Matt	329	798	160	106	146	23	63.5	12.57